Advanced Functional Materials

Dual-drug delivery using dextran-functionalized nanoparticles targeting cardiac fibroblasts for cellular reprogramming

--Manuscript Draft--

Manuscript Number:	adfm.201705134R1
Full Title:	Dual-drug delivery using dextran-functionalized nanoparticles targeting cardiac fibroblasts for cellular reprogramming
Article Type:	Full Paper
Section/Category:	
Keywords:	nanoparticles; small drug molecules; atrial natriuretic peptide; targeted drug delivery; heart
Corresponding Author:	Helder Santos, D.Sc. (Chem. Eng.) University of Helsinki Helsinki, Helsinki FINLAND
Additional Information:	
Question	**Response**
Please submit a plain text version of your cover letter here. **If you are submitting a revision of your manuscript, please do not overwrite your original cover letter. There is an opportunity for you to provide your responses to the reviewers later; please do not add them here.**	Irem Bayindir-Buchhalter Advanced Functional Materials Editor Dear Editor, We would like to submit our manuscript entitled “Dual-drug delivery using dextran-functionalized nanoparticles targeting cardiac fibroblasts for cellular reprogramming” by Mónica P.A. Ferreira, Virpi Talman, Giulia Torrieri, Dongfei Liu, Gonçalo Marques, Karina Moslova, Zehua Liu, João F. Pinto, Jouni Hirvonen, Heikki Ruskoaho, Hélder A. Santos for publication as a full paper in Advanced Functional Materials. Application of nanoparticles for the therapy of cardiac disease, such as myocardial infarction, is an emerging field and has shown potential benefits both in vitro and in animal models, bringing the technology closer to a potential clinical translation. As part of the therapeutic strategies of cardiac regeneration, the direct reprogramming of existent fibroblasts into cardiomyocytes has recently been explored by several research groups with the aim of developing the most efficient and safe way(s) to convert one cell type into another. Considering the poor water solubility of these innovative pharmaceutical agents, here we developed a dual drug-loaded functionalized AcDXSp-based nanoparticle, which promotes pH-dependently triggered drug delivery. The functionalization of the nanosystem improved its stability and biocompatibility, as well as provided higher specificity towards the cardiac cells. Finally, the intriguing observation of dual therapeutic effect reinforces the suitability of this nanosystem for pharmacologically-induced direct fibroblast reprogramming. Overall, as a proof-of-concept and for the first time, we have described the development of a biocompatible and functional nanodelivery system for pH-triggered delivery of at least two poorly-water soluble small drug molecules for applications promoting cardiac regeneration. This may be extended to other nanoparticulate-based systems and other small drug molecules. This work brings together several scientific areas, including materials science, biomedical engineering, biomaterials, dual-drug delivery, and cardiovascular diseases. This new result is completely covered within the scope of Advanced Functional Materials and is of timely interest to the readers of this journal. We firmly believe that this manuscript is suitable for publishing in Advanced Functional Materials. We truly declare that the present article and its contents have not been previously published in any language anywhere by any of the present authors and are not also

Powered by Editorial Manager® and ProduXion Manager® from Aries Systems Corporation

	under simultaneous consideration in another journal at the time of this submission. Thank you for your consideration. Sincerely yours, Hélder Santos Associate Professor Dr. Hélder A. Santos, D.Sc. (Chem. Eng.) Head of the Pharmaceutical Nanotechnology and Chemical Microsystems Unit Head of Preclinical Drug Formulation and Analysis Group Drug Research Program, Faculty of Pharmacy, University of Helsinki, Finland & Helsinki Institute of Life Science (HiLIFE), University of Helsinki, Finland @ email: helder.santos@helsinki.fi http://www.helsinki.fi/~hsantos/ https://scholar.google.com/citations?hl=en-EN&user=K3Pj_gwAAAAJ
Do you or any of your co-authors have a conflict of interest to declare?	No. The authors declare no conflict of interest.
Corresponding Author Secondary Information:	
Corresponding Author's Institution:	University of Helsinki
Corresponding Author's Secondary Institution:	
First Author:	Mónica Ferreira
First Author Secondary Information:	
Order of Authors:	Mónica Ferreira
	Virpi Talman
	Giulia Torrieri
	Dongfei Liu
	Gonçalo Marques
	Karina Moslova
	Zehua Liu
	João Pinto
	Jouni Hirvonen
	Heikki Ruskoaho
	Helder Santos, D.Sc. (Chem. Eng.)
Order of Authors Secondary Information:	
Abstract:	The inability of the heart to recover from an ischemic insult leads to the formation of fibrotic scar tissue and heart failure. From the therapeutic strategies under investigation, cardiac regeneration holds the promise of restoring the full functionality of a damaged heart. Taking into consideration the presence of vast numbers of fibroblasts and myofibroblasts in the injured heart, direct fibroblast reprogramming into cardiomyocytes using small drug molecules is an attractive therapeutic option to replenish the lost cardiomyocytes. Here, we developed a spermine-acetalated dextran-based functional nanoparticle for pH-triggered drug delivery of two poorly-water soluble small molecules, CHIR99021 and SB431542, both capable of increasing the efficiency of direct reprogramming of fibroblast into cardiomyocytes. Upon functionalization with polyethylene glycol and atrial natriuretic peptide, the biocompatibility of the nanosystem was improved, and the cellular interactions with the cardiac non-myocytes were specifically augmented. The dual delivery of the compounds was verified in vitro, and the compounds exerted concomitantly anticipated biological effects by stabilizing

Powered by Editorial Manager® and ProduXion Manager® from Aries Systems Corporation

	β-catenin (CHIR99021) and by preventing translocation of Smad3 to the nucleus of (myo)fibroblasts (SB431542). Our observations highlight the potential of this nanoparticle-based system towards improved drug delivery and efficient direct reprogramming of fibroblasts into cardiomyocyte-like cells, and thus, potential cardiac regeneration therapy.

Powered by Editorial Manager® and ProduXion Manager® from Aries Systems Corporation

WILEY-VCH

DOI: 10.1002/ ((please add manuscript number))
Article type: Full paper

Dual-drug delivery using dextran-functionalized nanoparticles targeting cardiac fibroblasts for cellular reprogramming

Mónica P.A. Ferreira, Virpi Talman, Giulia Torrieri, Dongfei Liu, Gonçalo Marques, Karina Moslova, Zehua Liu, João F. Pinto, Jouni Hirvonen*, Heikki Ruskoaho*, Hélder A. Santos**

[*] M. P. A. Ferreira, Giulia Torrieri, Dr. Dongfei Liu, Goncalo Marques, Zehua Liu, Prof. J. Hirvonen, Prof. H. A. Santos
Drug Research Program, Division of Pharmaceutical Chemistry and Technology, Faculty of Pharmacy, University of Helsinki, FI-00014 Helsinki, Finland
E-mail: monica.ferreira@helsinki.fi; Jouni.hirvonen@helsinki.fi; helder.santos@helsinki.fi

[*] Dr. V. Talman, Prof. H. Ruskoaho
Drug Research Program, Division of Pharmacology and Pharmacotherapy, Faculty of Pharmacy, University of Helsinki, FI-00014 Helsinki, Finland
Email: heikki.ruskoaho@helsinki.fi

G. Marques, Prof. J. F. Pinto
Faculty of Pharmacy, University of Lisbon, 1649-003 Lisbon, Portugal

Karina Moslova
Department of Chemistry, University of Helsinki, Helsinki FI-00014, Finland

[*] Dr. D. Liu, Prof. H. A. Santos
Helsinki Institute of Life Science, HiLIFE, University of Helsinki, FI-00014 Helsinki, Finland

Keywords: nanoparticles; small drug molecules; atrial natriuretic peptide; targeted drug delivery; heart

Abstract

The inability of the heart to recover from an ischemic insult leads to the formation of fibrotic scar tissue and heart failure. From the therapeutic strategies under investigation, cardiac regeneration holds the promise of restoring the full functionality of a damaged heart. Taking into consideration the presence of vast numbers of fibroblasts and myofibroblasts in the injured heart, direct fibroblast reprogramming into cardiomyocytes using small drug molecules is an attractive therapeutic option to replenish the lost cardiomyocytes. Here, we developed a spermine-acetalated dextran-based functional nanoparticle for pH-triggered drug delivery of two poorly-water soluble small molecules, CHIR99021 and SB431542, both capable of increasing the efficiency of direct reprogramming of fibroblast into cardiomyocytes. Upon functionalization with polyethylene glycol and atrial natriuretic peptide, the biocompatibility of the nanosystem was improved, and the cellular interactions with the cardiac non-myocytes were specifically augmented. The dual delivery of the compounds was verified *in vitro*, and the compounds exerted concomitantly anticipated biological effects by stabilizing β-catenin (CHIR99021) and by preventing translocation of Smad3 to the nucleus of (myo)fibroblasts (SB431542). Our observations highlight the potential of this nanoparticle-based system towards improved drug delivery and efficient direct reprogramming of fibroblasts into cardiomyocyte-like cells, and thus, potential cardiac regeneration therapy.

1. Introduction

Ischemic heart disease is the leading cause of death globally.[1] Myocardial infarction induces loss of up to one billion cardiomyocytes, and owing to the very limited regenerative capacity after injury,[2] the lost cells are replaced by a fibrotic scar tissue, leading to heart failure.[3] Although extensive efforts have been done to prevent, limit or treat heart failure, up to date there is still no treatment that could successfully restore the function of an injured heart. Gene therapy,[4] stem cell therapy with or without cardiac tissue engineering [5] or direct administration of proteins, pro-angiogenic cytokines [6] and transcription factors [7] have been reported as potential therapeutic alternatives. However, the effect of cardiac function in clinical trials of these interventions has been small or negligible, thus prompting to search for novel approaches.[8]

Recently, small drug molecules have been reported as being of potential use for cardiac regeneration purposes. Key compounds are, among others,[9] transforming growth factor-β type 1 receptor kinase (TGF-β) inhibitors, such as SB431542,[10] and Wnt activators, like CHIR99021.[11] TGF-β signaling pathway is involved in many biological processes, including cell proliferation, growth, development and differentiation. In fibroblasts, the early activation of the TGF-β pathway stimulates pro-fibrotic signaling, and this over-activation attenuates reprogramming of fibroblasts into beating cardiomyocytes.[12] Thus, inhibition of TGF-β pathway is important for cardiac fibroblast reprogramming. SB431542 is an activin receptor-like kinase (ALK) inhibitor. The TGF-β canonical signaling pathway involves the phosphorylation of Smads by ALKs, which is necessary for subsequent translocation to the nucleus for initiation of downstream signaling.[13] SB431542 inhibits the phosphorylation of Smads, thereby hampering their translocation to the nucleus.[14] Wnt/β-catenin signaling, on the other hand, has an important role in morphogenesis and differentiation during vertebrate heart development, and therefore it has been widely studied for differentiation of other cell types towards cardiac fate.[15] In the absence

of an active Wnt ligand, β-catenin is phosphorylated with a cytoplasmic complex of proteins, involving also the glycogen synthase kinase 3 (GSK3), leading to β-catenin degradation. In contrast, in the activated Wnt state, the destruction complex is inhibited, β-catenin is stabilized in the cytoplasm and translocated to the nucleus for regulating expression of target genes.[16] CHIR99021 is a potent inhibitor of the GSK3 and thereby activates β-catenin-regulated gene expression. Combinational therapies utilizing SB431542 and CHIR99021, as well as other small molecules, are efficient in inducing direct reprogramming of fibroblasts into cardiomyocyte-like cells,[14, 17] or in enhancing the proliferation of human induced pluripotent stem cell-derived cardiomyocytes,[11b] emphasizing the potential of small-molecule compounds in the development of cardiac regeneration-inducing therapies.

The application of micro- and nano-particulate systems for therapy of cardiovascular disease (CVD) is a relatively recent field, emerging as a promising alternative therapeutic and diagnostic approach.[18] These carriers serve as drug delivery vehicles for short-lived cytokines and growth factors, or/and for poorly water-soluble molecules, allowing a controlled release profile owing to the material features and tunable properties. The main advantages of the use of these drug carrier systems is the payload protection, prolongation and enhancement of the therapeutic effect of the intended drug compounds, along with lower drug administration frequency, and thus, improved patient compliance.[18-19] Examples of developed carriers include poly(lactide–co-glycolide) microparticles loaded with different growth factors alone or in combination, showing sustained release of the cargos, induction of cardiomyocyte proliferation and progenitor cell recruitment, attenuation of myocardial remodeling and improved cardiac function.[20]

Acetalated dextran (AcDX), known for being biocompatible, biodegradable, widely available and easily modified,[21] is an example of a polymer with pH-dependent drug delivery properties, for protein-based cargos applied in CVD therapy *in vivo* in the form of microparticles.[22] These AcDX microparticles were reported to produce tunable sustained release of cargos, cardioprotection, angiogenesis and reduction of

infarct area.[22] Yet, the disadvantage of the above-referred drug carrier systems is the need of invasive intramyocardial administration. Hence, it is important to address the administration route, reduce the drug carrier size to below the micrometer range and functionalize the particles in order to increase the chances of accumulation in the injured heart upon systemic administration.[23]

Direct reprogramming of fibroblasts has been identified as a potential therapeutic strategy for cardiac regeneration.[24] Hence, the aim of this study was to deliver concomitantly two poorly water-soluble model drugs, SB431542 and CHIR99021, which have been used in combination or with other compounds for direct reprogramming of fibroblasts into cardiomyocytes,[14, 17, 25] by encapsulating them inside the surface functionalized spermine-modified AcDX (AcDXSp) nanoparticles. We have previously demonstrated that atrial natriuretic peptide (ANP) functionalization of nanocarriers enhances their accumulation in the injured heart *in vivo*.[23] In addition, we have successfully applied AcDX for other therapeutic applications, such as cancer and immunotherapy.[26] In this study, we hypothesize that functionalizing the surface of AcDXSp with polyethylene glycol (PEG) can enhance the nanocarrier colloidal stability due to the intrinsic stealth properties of PEG,[27] while the functionalization with ANP can make the interaction of the nanocarrier more specific towards cardiac cells, due to the presence of natriuretic peptide receptors (NPR) on the cell membrane.[28] Additionally, the pH responsiveness of AcDXSp can provide a triggered release in the cytoplasm of cells upon internalization into the acidic subcellular compartments. The main goal of this study was to assess whether AcDXSp-based nanosystems could be used for targeting cardiac fibroblasts for cellular reprogramming applications.

2. Results and Discussion

2.1. Characterization of AcDX-based Nanosystems

The preparation of AcDXSp nanoparticles was performed by an oil-in-water (o/w) single emulsion method,[29] where the hydrophobic CHIR99021 (C) and SB431542 (S; combination of C and S abbreviated as CS), were incorporated in the organic phase with the AcDXSp polymer. For vehicle-loaded particles, similar conditions were used. As an aqueous phase, a solution of the stabilizer polyvinyl alcohol (PVA) was used, and upon the application of high energy sonication, the evaporation of the solvent occurred during 3 h. The drug-loaded and vehicle-loaded AcDXSp nanoparticles were further functionalized with PEG and ANP using crosslinking chemistry (**Scheme 1**), and their hydrodynamic diameter, polydispersity index (PdI) and zeta (ζ)-potential were evaluated by dynamic light scattering (DLS) and ζ-potential measurements (**Figure 1A**).

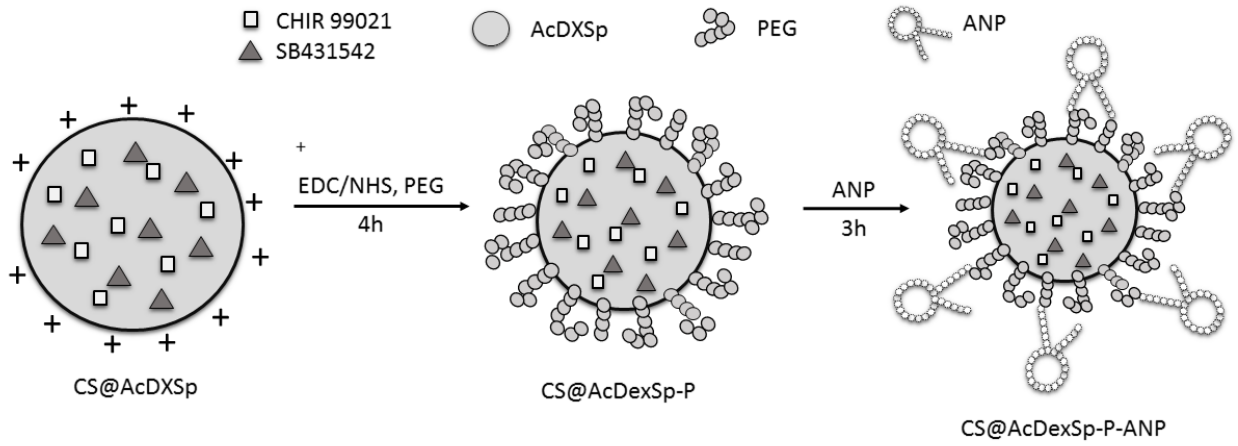

Scheme 1. Illustration of the PEG and ANP stepwise functionalization of drug-loaded AcDXSp prepared by an o/w single emulsion method using crosslinking chemistry. Not to scale.

The increase in size upon functionalization occurred similarly in both vehicle- and drug-loaded nanoparticles (**Figure 1A**), while their positive ζ-potential values, caused by the amine groups from the spermine functionalization, were slightly decreased due to the occupancy of $–NH_2$ and the presence of –

COOH moieties present at the end parts of PEG (AcDXSp-P). Further functionalization with ANP (AcDXSp-P-ANP) maintained or slightly decreases the ζ-potential values of the nanosystems due to the occupancy of ANP amine groups with the covalently attached PEG. For simplification, the loaded nanoparticles are abbreviated as CS@AcDXSp, CS@AcDXSp-P and CS@AcDXSp-P-ANP. The presence of PEG at the surface of AcDXSp functionalized nanoparticles was evaluated by attenuated total reflectance Fourier transform infrared (ATR−FTIR) spectroscopy (**Figure 1B**). The appearance of amide-indicative bands at 1565–1570 cm^{-1} (in-plane N−H bending and C−N stretching) and 1630–1640 cm^{-1} (amide C=O stretching) confirmed the formation of a covalent amide bond between the AcDXSp and PEG, and the appearance of a shoulder at 1735 cm^{-1} (C=O stretching from –COOH) denotes the presence of free carboxyl groups. The further functionalization with ANP did not show modifications in the FTIR spectrum. Elemental analysis of AcDXSp-P and AcDXSp-P-ANP nanoparticles showed the presence of about 4.8 ± 1.7 μg of ANP in 1 mg of AcDXSp-P-ANP nanoparticles, confirming the successful functionalization.

Because the *in vitro* studies were all performed in cell culture medium, we evaluated the colloidal stability of the nanosystems also in culture medium. While AcDXSp nanoparticles display a progressively growing hydrodynamic diameter, upon stabilization with PEG this parameter remains constant over time for both AcDXSp-P and AcDXSP-P-ANP (**Figure 1C**). This demonstrates the stealth properties generated by the PEG coating.[27] The PdI remained satisfactorily stable with a non-significant raise in the values for ANP-functionalized nanoparticles (**Figure 1D**). As observed and demonstrated in other studies, PEGylation is necessary for the stabilization of the nanoparticles and for the prolongation of the blood circulation time, mainly because it provides a hydrophilic coating, and at the same time its flexible structure creates steric hindrance towards interactions with neighboring objects.[30]

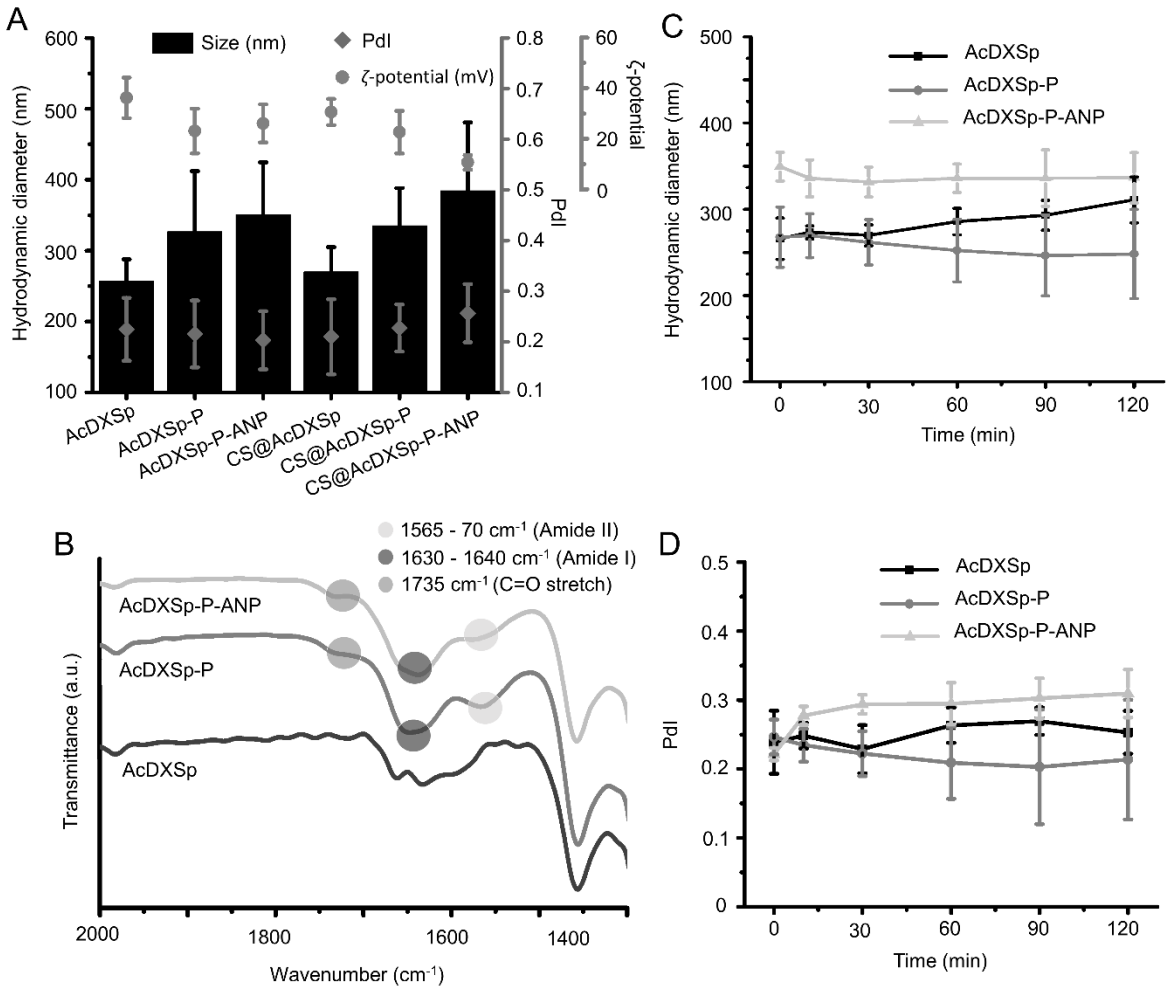

Figure 1. Physicochemical characterization of AcDXSp nanoparticles before and after surface functionalization. (A) Hydrodynamic diameter, PdI, and ζ-potential of AcDXSp, AcDXSp-P and AcDXSp-P-ANP nanoparticles, as well as the drug-loaded CS@AcDXSp, CS@AcDXSp-P and CS@AcDXSp-P-ANP in Milli-Q water (pH > 8). Values are represented as the mean ± standard deviation (s.d.) ($n \geq 3$). (B) ATR−FTIR spectra of AcDXSp, AcDXSp-P and AcDXSp-P-ANP nanoparticles. Upon surface modification with both PEG and ANP, it was observed the appearance of the amide I and II bands at 1630–1640 cm^{-1} and 1565–1570 cm^{-1}, respectively, indicating the presence of covalent amide bonds. The appearance of a band at 1716 cm^{-1} (carbonyl C=O stretching) in the AcDXSp-PEG spectrum reveals the presence of free carboxyl groups for further ANP attachment, slightly attenuated upon the addition of ANP. The spectra were normalized for clarification. (C–D)

Evaluation of the impact of cell medium on the colloidal stability of AcDXSp, AcDXSp-P and AcDXSp-P-ANP nanoparticles upon incubation for 120 min at 37 °C. The results were calculated from the DLS measurement data as a function of time, and are represented as the mean ± standard deviation (s.d.) ($n \geq 3$).

2.2. pH-Dependent Degradation and Drug Release

To assess the pH-dependent degradation behavior of the polymeric matrix, we incubated each nanosystem in physiologically relevant buffer solutions at pH 5 and 7.4, which simulate the conditions inside the cellular acidic compartments [31] and the extracellular environment, respectively. **Figure 2A** shows the degradation behavior of the different nanosystems, and only mild alterations in their integrity were noted at pH 7.4, which are reflected in the release profile of the cargos in **Figures 2B** and **2D**. On the other hand, the disintegration of the nanoparticle structure occurred much faster at pH 5, which is in line with a faster release of the cargos (**Figures 2C** and **2E**). These observations are in agreement with the widely described pH-dependent hydrolysis rate features of the acetal groups of the acetalated dextran.[32] Altogether, the TEM images of the different nanosystems (**Figure 2A**), along with with the DLS data (**Figure 1A**), confirm the observations of minimal particle decomposition upon functionalization, and are in agreement with the progressive size increase observed in DLS measurements.

Two reprogramming molecules, CHIR99021 and SB431542, were encapsulated into the polymeric AcDXSp matrix, which was further surface functionalized. The compound concentrations and molar ratios (approximately 1:2) were based on testing different concentrations in non-myocytes (data not shown). The encapsulation efficiency (EE) and loading degrees (LD) of bare and functionalized nanoparticles are shown in **Table S1**. Even though the surface modifications were performed at pH values close to 8, there is a decrease in both EE and LD from bare to functionalized AcDXSp

nanoparticles. A possible explanation for this leakage is that despite extensive washing, small amounts of drug may still remain on the surface of the nanoparticles. Moreover, the polymeric matrix might be saturated, possible due to the excessive amounts of cargos used to encapsulate inside the polymeric matrix. The same phenomenon has been described for siRNA encapsulation inside AcDXSp particles.[32c] As the IC_{50} values of the compounds are in the nanomolar range, we however anticipated (and subsequently showed, see below) that the LD attained was sufficient to produce biological responses.[33] To evaluate the pH-dependent release from the bare and functionalized drug-loaded nanoparticles, dissolution studies were performed at both pH 7.4 and 5 in sink conditions, and the free drugs were used as controls. While the free compounds demonstrated pH-dependent dissolution profiles, their release profiles in both conditions were similar and dictated by the degradation hydrolysis of the polymeric matrix towards mildly acidic conditions.[32a] As expected, the release occurred much faster at pH 5 compared to pH 7.4 (**Figure 2B–2E**). The small amounts of cargos released at pH 7.4 are justifiable by a slight degradation of dextran at this pH resulting in release of a small percentage of the cargos, as previously reported.[34] After functionalization of the nanoparticles, a slightly faster drug release at pH 7.4 can be noted than for the bare AcDXSp nanoparticles, possibly due to the more hydrophilic surface of the functionalized nanoparticles, which facilitated the interaction with the solvent molecules and released the cargos entrapped closer to the surface. In addition, the obtained degree of acetalation of 46.1% for the AcDX molecule also influenced on the low drug release observed at pH 7.4, because the higher is the acetalation of AcDX, the lower is the degradation rate of the polymeric matrix at pH-values above 6.0.[22a] Furthermore, substantial amounts of both cargos were rapidly released within the first hour at pH 5. The dissolution rate of both drugs is therefore improved in mildly acidic conditions, and the release of both cargos is precisely triggered only upon acidic pH stimulus. These properties have previously been described also for other poorly water-soluble drugs.[35] Considering nanoparticles for intravenous administration, this is an optimal condition, since the cargo will only be released upon

internalization into acidic subcellular compartments in the cells of the target tissue. In addition, the ischemic myocardium presents inflammation and consequently changes in the interstitial pH to 6 – 6.5, [36] which makes this polymer a high-quality candidate for sustained drug delivery to the injured myocardium, as previously reported.[22]

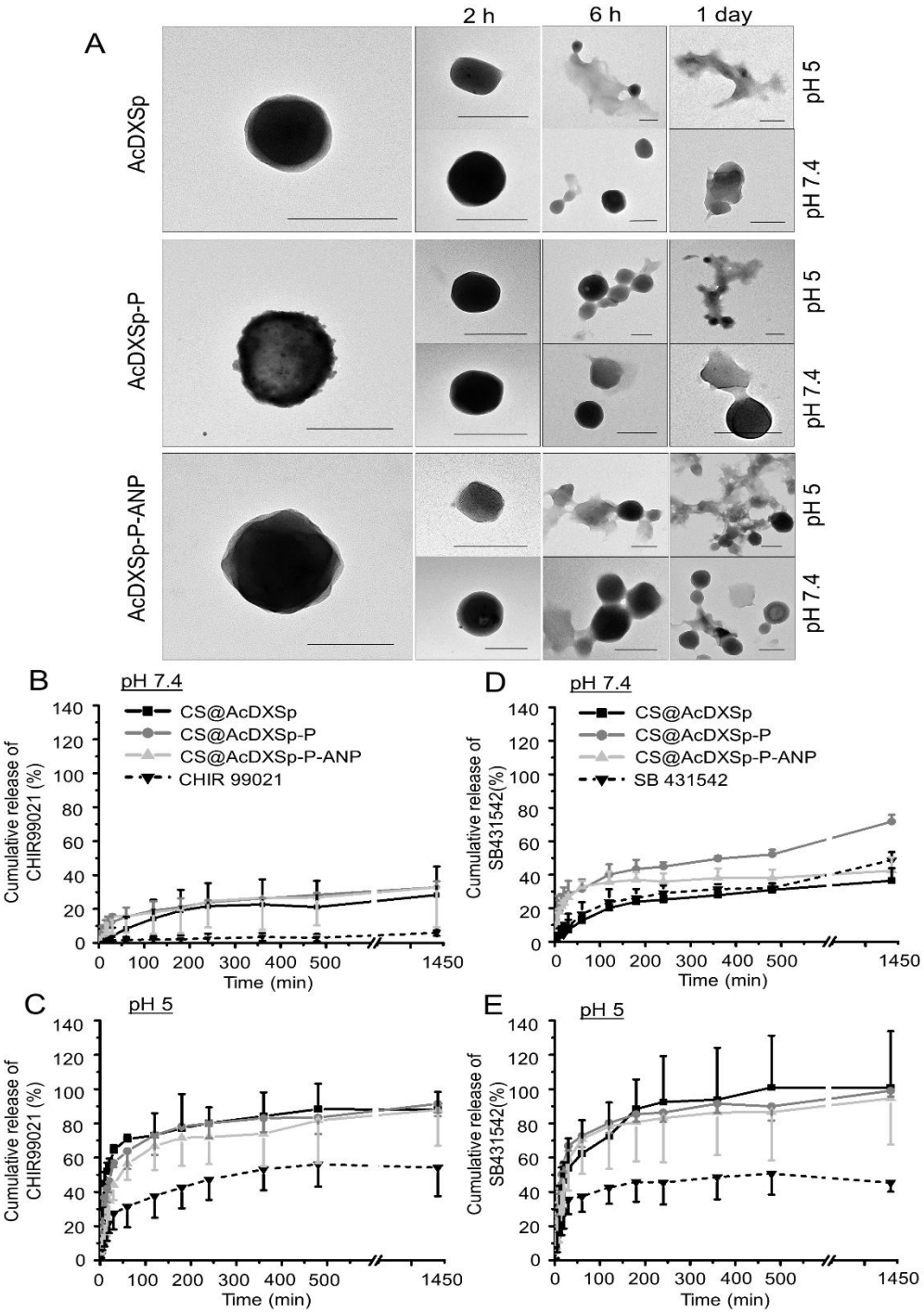

Figure 2. Degradation and drug release profiles of the AcDXSp nanoparticle preparations. (A) TEM images of the structural morphology of AcDXSp, AcDXSp-P and AcDXSP-P-ANP nanoparticles for time points 0, 2 h, 6 h and 1 day, incubated in simulated extracellular (pH 7.4) and intracellular (pH 5) conditions. The degradation process of the AcDXSp matrix occurred faster at pH 5.0. Scale bars are 23 nm. (B–E) The release profiles of CHIR99021 (B, C) and SB431542 (D, E) from bare CS@AcDXSp and functionalized CS@AcDXSp-P and CS@AcDXSp-P-ANP, evaluated at pH 7.4 and 5.0, at 37 °C. Data represent mean ± s.d. ($n \geq 3$).

2.3. Cytocompatibility and Cell–Nanoparticle Interactions

The cytocompatibility of the nanosystems was evaluated in primary cardiac cells. Non-myocytes were starved with serum-free medium for 18 h prior to treatments in order to suppress extensive activation of the signaling routes investigated,[37] and serum-free conditions were maintained during the incubation with nanoparticles. Cardiac non-myocytes demonstrated a dose-dependent decrease in cell viability when incubated with bare vehicle-loaded and drug-loaded AcDXSp nanoparticles (**Figure 3**). Such observations were expected due to the highly cationic nature of the bare AcDXSp nanoparticles and the presence of the oligoamine spermine. The positively charged nanoparticle surface readily interacts with the negatively charged cell membrane, promoting high cell–nanoparticle interactions and internalization. However, this kind of behavior is also known to induce cell toxicity by causing disruption of membrane integrity; damage of intracellular compartments such as mitochondria and formation of autophagosomes.[38] PEGylation diminished the toxicity: no toxicity was observed even at the highest particle concentrations (250 µg/mL) with PEGylated and ANP-functionalized nanoparticles. This is due to the intrinsic hydrophilicity and bioinert properties of PEG.[39] We also evaluated the cytocompatibility of these nanosystems in cardiomyocytes (**Figure S1**). Cardiomyocytes were more resistant to the cationic AcDXSp nanoparticles compared to non-myocytes, while a concentration dependent toxicity was

observed for PEGylated and ANP-functionalized nanoparticles. This might be explained by the presence of bovine serum albumin in the cardiomyocyte culture medium, which might have interacted with the positively charged AcDXSp nanoparticles and hided their positive surfaces, thus preventing cell–nanoparticle interactions. It has been extensively described that protein adsorption onto nanoparticle surface impacts the way the nanoparticles interact with cells.[40] Upon PEGylation, protein−nanoparticle interactions are reduced, which preserves their native surface and favors possible interactions, consequently inducing some degree of toxicity, as PEGylated and ANP-functionalized nanoparticles are mildly cationic. We have previously observed higher resistance of cardiomyocytes against the treatment with positively-charged nanoparticles than was the case with non-myocytes.[23] In summary, our functionalized nanosystems revealed to be more cytocompatible with non-myocytes even at high concentrations, while for cardiomyocytes, the lower concentrations were less toxic.

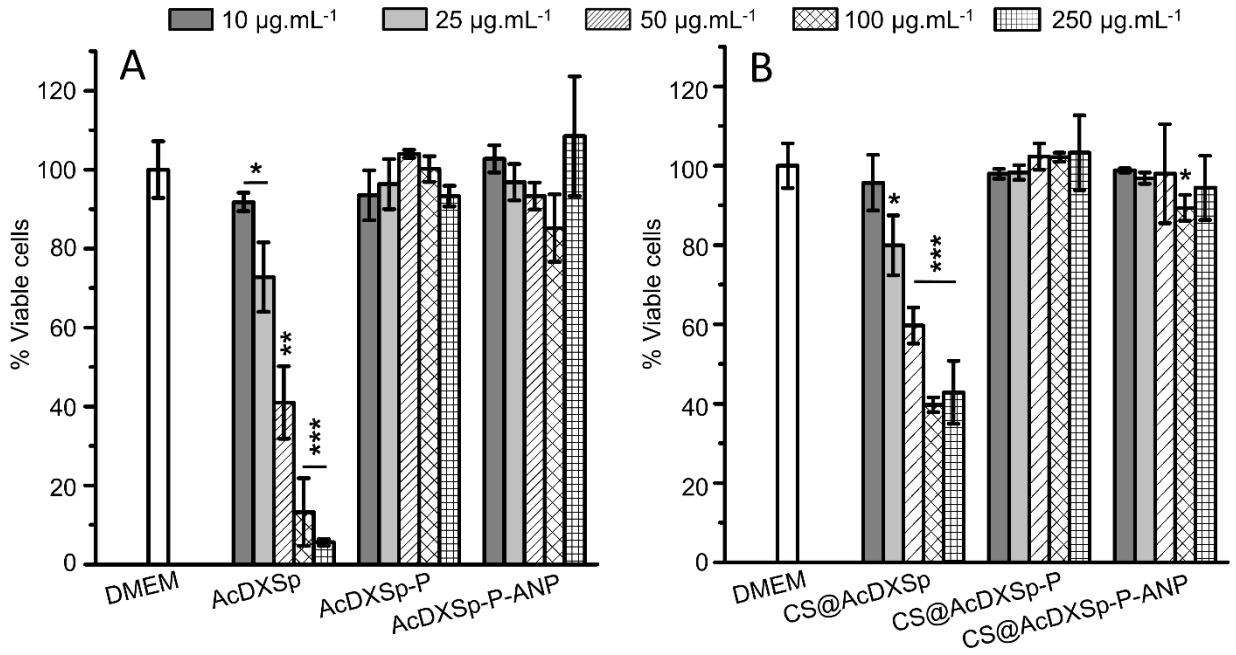

Figure 3. Effects of nanoparticle preparations on the viability of cardiac non-myocytes. Cell viability of primary non-myocytes, as determined by measuring the ATP content of actively metabolic

cells after incubation for 6 h with vehicle-loaded (A) and drug-loaded (B) nanoparticles at concentrations of 10–250 µg/mL. A Student *t*-test was used for the statistical analysis. The results are presented as the mean ± s.d. ($n \geq 3$). The levels of significance were set at probabilities of $^{*}p < 0.05$, $^{**}p < 0.01$, and $^{***}p < 0.001$, compared with the cell medium-treated control (DMEM).

The role of ANP at the nanocarrier surface is to promote a more specific interaction with the cardiac cells, because they express all types of NPRs at the cell membrane level.[28b, 41] Therefore, we investigated the cellular interactions with the different nanosystems by incubating non-myocytes with Alexafluor488®-labelled nanoparticles during 1 h (**Figure 4**). Quenching of the fluorescence was done to analyze the extent of internalized nanoparticles. As expected, the interactions between cells and nanoparticles occurred quickly for all formulations due to the cationic surface properties. Even though the bare and PEGylated AcDXSp nanoparticles showed similar median fluorescence intensity (MFI) values, upon fluorescence quenching, the AcDXSp nanoparticles were internalized to a higher extent than the PEGylated and ANP-functionalized nanoparticles (**Figures 4B** and **4C**). Because of the highly positive surface charge, AcDXSp nanoparticles interact readily and unspecifically with the cell membrane. This is in agreement with the cell viability results (**Figure 3**) and observations related with positive surfaces and enhanced cell interactions.[38] The presence of PEG in the nanoparticles decreased the positive charge, enhanced the hydrophilicity of the nanoparticle surface, and thus, to some extent reduced the unspecific cell interactions and cell uptake, at the same time improving the cytocompatibility. The cellular association showed to be significantly more prominent for the ANP-functionalized nanoparticles compared to the bare and PEGylated nanoparticles. This interaction was further displaced when free ANP was added into the culture medium, indicating that the nanoparticle functionalization with ANP enhanced the specificity of the cell–nanoparticle interactions. The same trend was observed upon quenching, showing that the free ANP prevented AcDXSp-P-ANP particle uptake by the cells

(**Figures 4A** and **4C**). This is due to the presence of NPR in the non-myocyte cell membrane, as the free ANP will compete with the AcDXSp-P-ANP nanoparticles to bind to the NPRs, thus displacing the specific cell−nanoparticle interactions, as described in our previous study.[23] Not ruling out the possibility of passive targeting due to the small particle size of our nanoparticles [42] and the presence of enhanced vascular permeability in the injured myocardium,[43] these properties could represent an advantage upon intravenous injection, due to an increased blood circulation and specific cell interaction mediated by NPRs, increasing the probability of nanoparticle accumulation in the injured myocardium and leading to a more directed drug delivery.

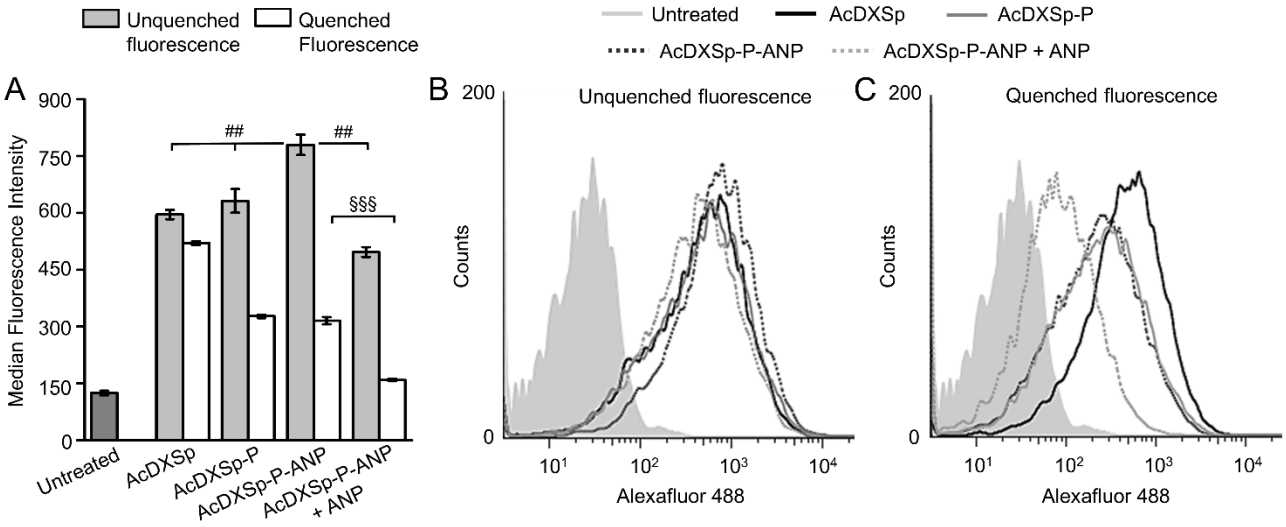

Figure 4. *In vitro* quantitative cellular interaction studies. (A) Flow cytometry results for serum-starved non-myocytes after 1 h incubation with Alexafluor488®-labelled nanoparticles (25 µg/mL). Median fluorescence intensity values of untreated cells (grey), nanoparticle-treated cells before quenching (pink) and after quenching (blue) the fluorescence at the cell surface. (B) Histograms of non-quenched and (C) quenched fluorescence at the cell surface for untreated and nanoparticle-treated cells. Untreated (dotted line), AcDXSp nanoparticles (black), AcDXSp-P (grey), AcDXSp-P-ANP (blue) and AcDXSp-P-ANP + free ANP (100µM) (pink). Approximately 10,000 events were counted for each

measurement. Values represent the mean ± s.d. (n = 3). A one-way ANOVA followed by a Tukey-Kramer post hoc test was used for the statistical analysis. The significance levels of the differences were set at probabilities of $^{\#\#}p < 0.01$ for comparison with AcDXSp-P-ANP (before fluorescence quenching) and $^{\S\S\S}p < 0.001$ for comparison between AcDXSp-P-ANP AcDXSp-P-ANP + free ANP (upon fluorescence quenching).

2.4. Modulation of Wnt and TGF-β signaling pathways in cardiac fibroblasts

In order to address the main goal of this study, the potential use of nanoparticulate systems for direct fibroblast reprogramming, we incubated pre-starved non-myocytes with drug-loaded AcDXSp-functionalized nanoparticles. As controls, both vehicle-loaded nanoparticles and the free compounds were used. In all the conditions where the compounds were present, 1 µM of CHIR99021 and 2.1 µM of SB431542 were used in all the tests, correspondent to a safe dose of nanoparticles given, which was calculated based on the LD of the different nanoparticles. The biological effect was assessed by quantifying the staining intensity for β-catenin and Smad3. After a 6-h incubation with nanoparticles, the cells were immunostained for nuclei (4',6-diamidino-2-phenylindole dihydrochloride, DAPI), β-catenin or Smad3, and in addition, for a fibroblast marker, vimentin or α-smooth muscle actin (SMA), which demonstrated that the majority of cardiac non-myocytes were (myo)fibroblasts (**Figures 5A** and **5E**). The quantification of Smad3 and β-catenin intensity was done using high content imaging from regions of interest corresponding to the nucleus and the cytoplasm (DAPI staining was used to define the nuclear area and a 5-pixel ring immediately outside the nucleus was considered to represent cytoplasm). The results are presented in **Figures 5**.

The nanoparticles loaded with Wnt activator CHIR99021 enhanced β-catenin stabilization when compared to the untreated group and the vehicle-loaded nanoparticles ($p < 0.05$). This led to an increase

of β-catenin in the cytoplasm, as well as in the nucleus (**Figures 5B** and **5C**). Importantly, the effect of CHIR90221 on stabilization of β-catenin in the cytoplasm was significantly higher for CS@AcDXSp-P-ANP compared with the free drug ($p < 0.05$), indicating improvement in the delivery of CHIR99021 by the ANP-functionalized nanoparticles. The nucleus to cytoplasm ratio of β-catenin did not differ significantly among groups, except for the CS group, in which to the cytoplasmic β-catenin appeared to be lower than in the drug-loaded nanoparticle groups (**Figures 5C** and **5D**). Overall, these observations demonstrate the suitability of the functionalized nanoparticulate systems to deliver intracellularly the poorly water-soluble drug CHIR99021.

The delivery of the TGF-β inhibitor SB431542 affected the intracellular Smad3 by preventing its translocation to the nucleus, while it did not seem to interfere with the amount of Smad3 already existent in the nucleus for the 6 h (**Figure 5F**). This is in agreement with the mechanism of action of the compound, since it prevents the phosphorylation of Smad3 by the ALK and the consequent Smad complex formation for nuclear translocation.[13] Although free SB431542 significantly increased the cytoplasmic Smad3 compared to its control ($p < 0.05$, CS *vs.* DMSO), this effect was more marked for the drug-loaded nanoparticles, as reflected by the statistically significant cytoplasmic increase of Smad3 compared to all the other groups, including the CS group (**Figure 5G**, $p < 0.05$). This effect was also noted in the ratio of nuclear/cytoplasmic Smad3 staining intensity (**Figure 5H**).

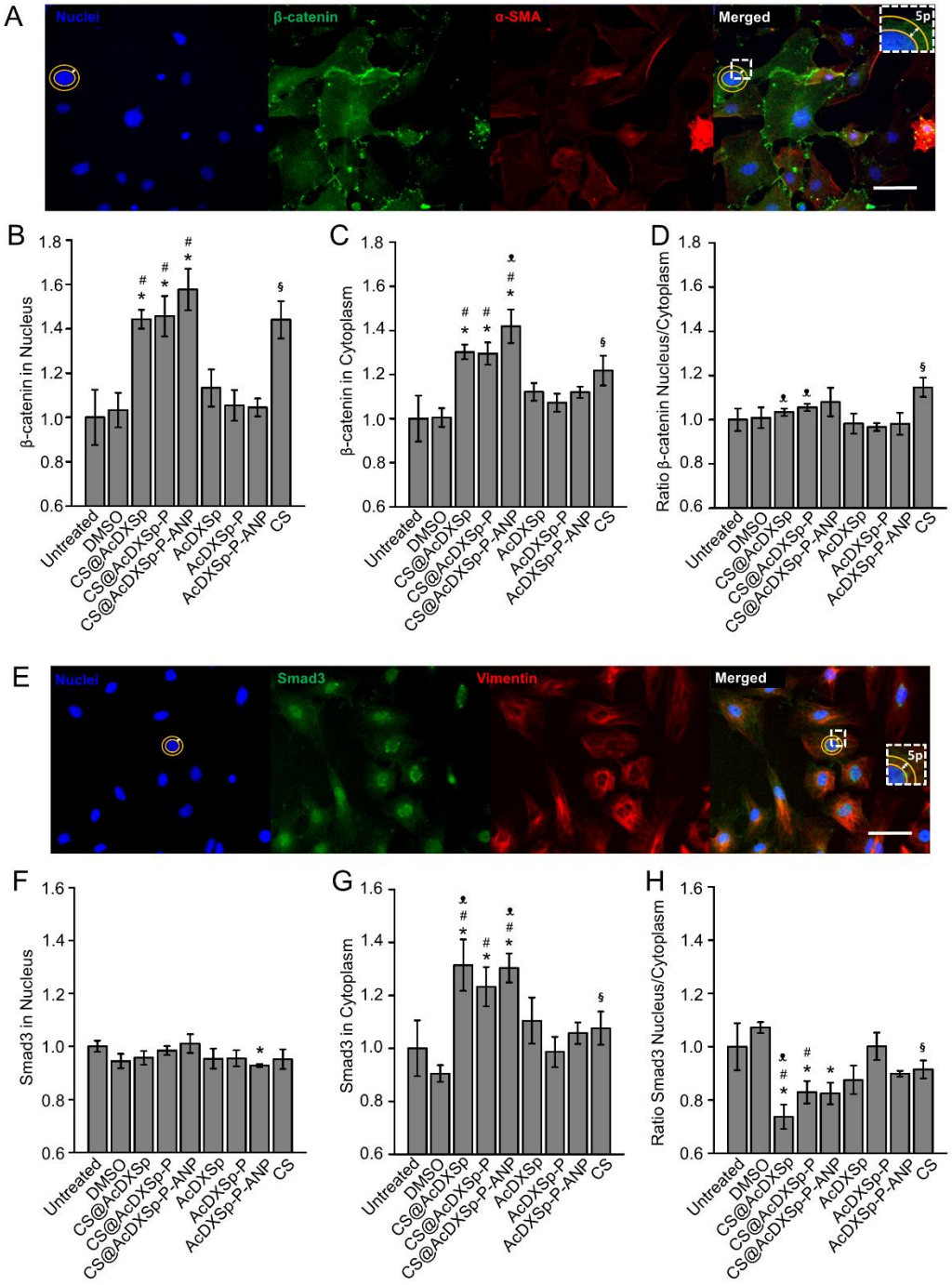

Figure 5. High-content cell imaging and quantification of β-catenin and Smad3 staining intensity and sub-cellular localization. (A) Representative images of non-myocyte cells treated with CS@AcDXSp-P-ANP at the concentrations of 1 μM of CHIR 99021 and 2.1 μM of SB 431542, and stained for nuclei (DAPI, blue), β-catenin (green) and the myofibroblast marker α-smooth muscle actin

(α-SMA, red), with a 20× magnification objective. Scale bars are 50 µm. (B-D) Quantification of β-catenin staining intensity: the average intensity of β-catenin staining in the nucleus (B), in the cytoplasm (C) and the ratio of β-catenin in nucleus/cytoplasm (D). (E) Representative images of non-myocyte cells treated with CS@AcDXSp-P-ANP at the dose of 1 µM of CHIR 99021 and 2.1 µM of SB 431542, and stained for nuclei (DAPI, blue), Smad3 (green) and the fibroblast marker, vimentin (red), with a 20× magnification objective. (F–H) Quantification of Smad3 staining intensity: the average intensity of Smad3 staining in the nucleus (F), in the cytoplasm (G) and the ratio of Smad3 in nucleus/cytoplasm (H). The different treatment conditions are stated below each bar. The fluorescence intensity in the cytoplasm was quantified from a 5-pixel ring immediately outside the nucleus defined by DAPI staining, as indicated for one cell in panel A. The data was normalized to the untreated control. A one-way ANOVA followed by a Tukey-Kramer post hoc test was used for the statistical analysis. The significance levels of the differences were set at probabilities of $^{*}p < 0.05$ for comparison with untreated; $^{\#}p <$ for comparison between drug-loaded *vs.* vehicle-loaded nanoparticles; $^{\S}p < 0.05$ for comparison between DMSO and CS groups and $^{\bullet}p < 0.05$ for comparison of loaded nanoparticles *vs.* CS group. Values represent the mean ± s.d. ($n = 3$).

The use of nanoparticulate systems for drug delivery applications has shown numerous advantages in multidisciplinary biomedical fields. Delivery of small molecules, growth factors and nucleic acid cargos to the heart with the particulate systems using diverse strategies have been described.[18, 19b, 20, 22a, 23, 44] However, employment of particulate systems for the application of direct cardiac reprogramming is scarce and involves generally the delivery of microRNAs and viral vectors.[45] The use of small drug molecules for direct cardiac reprogramming is an emerging research field, yet efforts towards its clinical translation are limited or even nonexistent.[46] Due to the poor water solubility of CHIR99021 and

SB431542, we took the advantage of the beneficial properties of nanoparticulate systems to improve the delivery of these compounds with reported potential to enhance direct cardiac reprogramming, and thus, overcome the drawbacks of reprogramming techniques using multiple genetic factors with low efficiency, technical and safety issues.[4d, 12, 14, 24b, 24c, 47] Several reports on the combined application of CHIR99021 and SB431542 for cardiac fibroblasts reprogramming specifically justified the concomitant use of both the compounds in this study to be delivered simultaneously by a functional nanoparticulate system. In addition, this functional nanosystem could potentially be also explored for induction of cardiomyocyte proliferation, because the inhibition of GSK-3 (involved in degradation of β-catenin) may induce cell proliferation and mitosis in cardiomyocytes as previously described.[48] Overall, to our knowledge, this is the first study demonstrating the potential delivery of key small-molecule drugs using targeted nanoparticulate systems for the purpose of direct reprogramming of cardiac fibroblasts into cardiomyocytes, and the potentialities for nanoparticulate carriers for applications in cardiac regeneration are only now starting to be explored.

3. CONCLUSIONS

Application of nanoparticles for the therapy of cardiac disease, such as myocardial infarction, is an emerging field and has shown potential benefits both *in vitro* and in animal models, bringing the technology closer to a potential clinical translation. As part of the therapeutic strategies of cardiac regeneration, the direct reprogramming of existent fibroblasts into cardiomyocytes has recently been explored by several research groups with the aim of developing the most efficient and safe way(s) to convert one cell type into another. Considering the poor water solubility of these innovative pharmaceutical agents, here we developed a dual drug-loaded functionalized AcDXSp-based nanoparticle, which promotes pH-dependently triggered drug delivery. The functionalization of the nanosystem improved its stability and biocompatibility, as well as provided higher specificity towards the cardiac cells. Finally, the intriguing observation of dual therapeutic effect reinforces the suitability of this nanosystem for pharmacologically-induced direct fibroblast reprogramming. Overall, as a proof-of-concept and for the first time, we have described the development of a biocompatible and functional nanodelivery system for pH-triggered delivery of at least two poorly-water soluble small drug molecules for applications promoting cardiac regeneration. This may be extended to other nanoparticulate-based systems and other small drug molecules.

4. Experimental section

Synthesis of AcDX and Modification with Spermine. Dextran (5 g, MW 9–11 kDa; Sigma-Aldrich, USA) was dissolved into 20 mL of Milli-Q water. Sodium periodate (0.22 g; Sigma-Aldrich, USA) was added to the dextran solution and the mixture was stirred at room temperature for 5 h to yield partially oxidized dextran. Dialysis was used to purify the partially oxidized dextran against distilled water, using a regenerated cellulose membrane (Spectra/Por RC tubin, MWCO 3.5 k). Upon lyophilization, partially

oxidized dextran (3 g) was modified with 2-methoxypropene (10.6 mL, Sigma–Aldrich, USA) and pyridinium p-toluenesulfonate (46.8 mg; Sigma–Aldrich, USA) in anhydrous dimethyl sulfoxide (30 mL, Sigma–Aldrich, USA) during 1 hour under a N_2 atmosphere to obtain the partially oxidized AcDX, as described elsewhere [26a, 49]. Triethylamine (TEA, 1 mL; Sigma–Aldrich, USA) was used to quench the reaction. The resulting product was precipitated in and centrifuged (10 min, 68320*g*). The pellet was washed twice with H_2O and dried in vacuum at 40 °C during 48 h. Partially oxidized AcDX (2.0 g) was dissolved in 20 mL of DMSO and spermine (4.0 g, 19.8 mmol; Sigma-Aldrich, USA) was added to the solution and kept stirring for 24 h at 50 °C. Sodium borohydride ($NaBH_4$, 1.0 g; Sigma-Aldrich, USA) was added and the reduction reaction was allowed to occur at room temperature at least for 24 h. Methanol (10 mL) and Milli-Q water (80 mL) were added to the flask to precipitate the polymer and to dissolve the excess $NaBH_4$. The polymer was washed with Milli-Q water (5 × 180 mL, pH 8). Residual moisture was removed by lyophilization, yielding white spermine-modified AcDX (AcDXSp) powder.[32c] The degree of functionalization was determined by ^{1}H NMR spectroscopy in DCl/D_2O according to the method. ^{1}H NMR (400 MHz, CDCl3): δ 1.40 (s, br, acetal), 3.25 (br, acetal), 3.45, 3.50−4.10, 4.90, 5.10 (br, dextran).

Preparation of AcDXSp Nanoparticles. AcDXSp nanoparticles were prepared by an o/w single emulsion method. AcDXSp polymer (6.5 mg) was dissolved in CH_2Cl_2 (0.125 mL). The compounds CHIR99021 (300 µg, Tocris, UK) and SB431542 (500 µg, Sigma) were added to the AcDXSp solution. An aqueous solution of PVA (M_W: 31000−50000 g/mol, Sigma) (0.25 mL, 2.0%, w/v) was further added, the mixture was mixed thoroughly and emulsified by sonication during 30 s on ice, with an output setting of 5 and a duty cycle of 50%, using a probe sonicator (Sonics VCX 750, USA). The resulting o/w emulsion was transferred immediately to another solution of PVA (0.75 mL, 0.2% w/v) and stirred for 3 h to allow evaporation of the CH_2Cl_2 solvent at room temperature. The resulting CS@AcDXSp nanoparticles were

pelleted by centrifugation (16100*g*, 5 min), washed twice with Lutrol® F127 0.5 % pH 8 (BASF) and once with Milli-Q. All supernatants were kept for detection of CHIR99021 and SB431542 content by HPLC. Vehicle-loaded nanoparticles were prepared similarly.

Surface Modification of AcDXSp Nanoparticles. The surface of the AcDXSp nanoparticles was modified with PEG (CO_2H-PEG-CO_2H, M_W: 2000 g/mol, Sigma-Aldrich, USA) and atrial natriuretic peptide (ANP, M_W: 3080 g/mol, United BioSystems Inc, USA), following a protocol previously described [50] using crosslinking chemistry with slight modifications. A solution of 1-ethyl-3-(3-dimethylaminopropyl)carbodiimide hydrochloride/N-hydroxysulfosuccinimide (EDC/NHS, Sigma-Aldrich, USA) was prepared by adding 8 µL of EDC and 2 mg of NHS to 2 mL of 10 mM 2-(N-morpholino)ethanesulfonic acid (MES, Sigma-Aldrich, USA). The pH was adjusted to 7.8. PEG (20 mg) was first added to the EDC/NHS solution and the AcDXSp nanoparticles (2 mg) were then suspended in the same solution, in an optimized ratio of 1:10 (AcDXSp:PEG), stirring at room temperature during 4 h in dark. AcDXSp-P nanoparticles were pelleted by centrifugation (16100*g*, 5 min) and the supernatant discarded. AcDXSp-P were resuspended in a solution of ANP in MES pH 8 (3.6 mg/mL) and kept under stirring during 3 h at room temperature, in dark. The resulting AcDXSp-P-ANP nanoparticles were washed twice with sucrose 2% (pH 8). For fluorescence labeling, AcDXSp were activated using EDC/NHS chemistry and AlexaFluor488® (500:1 AcDXSp:AF488, w/w) during 1 h. PEGylation and modification with ANP were performed, as described above.

Physicochemical Characterization. The hydrodynamic diameter and polydispersity index (PdI) were measured in a disposable polystyrene cuvette (SARSTEDT AG & Co., Germany) by DLS, while ζ-potential was measured in a disposable folded capillary cell (DTS1070, Malvern, UK) using a Zetasizer Nano ZS instrument (Malvern Instruments Ltd., UK). The surface chemical composition of the dry nanoparticles was evaluated by ATR–FTIR using a Bruker VERTEX 70 series FTIR spectrometer (Bruker Optics, Germany) and an ATR sampling accessory (MIRacle, Pike Technology, Inc.). The ATR–

FTIR spectra were recorded in the wavenumber region of 4000–650 cm^{-1} with a resolution of 4 cm^{-1} at room temperature, using OPUS 5.5 software. The spectra were normalized between 0 and 1 for clarification. The amount of ANP covalently conjugated onto AcDXSp-PEG nanoparticles was determined by elemental analysis using a vario MICRO cube CHNS analyzer (Elementar AnalysenSystem) in dry samples. The percentages of carbon, hydrogen and nitrogen were recorded. The amount of ANP conjugated onto the nanoparticles' surface was calculated based on the percentage of each element and the chemical structure of ANP. The nanoparticles' morphology was evaluated by transmission electron microscopy (TEM, Jeol JEM-1400, Jeol Ltd., Japan). The samples were prepared by immersion of the carbon-coated copper grids (300 mesh; Electron Microscopy Sciences, USA) into a suspension of 0.1 mg/mL of the nanocarrier suspensions during approximately 1 min, blotted away and left to dry at room temperature overnight. To evaluate their dissolution behavior under different pH-conditions, the AcDXSp nanoparticles, AcDXSp-P and AcDXSp-P-ANP were individually added into the buffer solution (pH 7.4 and 5.0) at a concentration of 1 mg/mL. Samples were taken at different time points (100 µL) to a TEA solution (0.01%, v/v; 1 mL, pH 8) to terminate the degradation process of AcDXSp, centrifuged (5 min, 16100*g*), and redispersed in TEA solution (0.01%, v/v; pH 8). The sample preparation for TEM imaging was similar to the described above.

High-performance liquid chromatography (HPLC), determination of encapsulation efficiency (EE), loading degree (LD) and drug release tests. An Agilent 1100 series HPLC system (Agilent Technologies, Germany) was used to quantify the compounds encapsulated inside the nanoparticles. A Discovery® 5 µm C_{18} reversed phase column (100 × 4.6 mm, Supelco, USA) was used. The mobile phase was Na_2HPO_4:citric acid (2:1) (pH 6.0) and acetonitrile (ACN) (50:50, *v/v*). The flow rate used was 1.4 mL/min, the injection volume 5 µL, and the wavelength 274 ± 20 nm. For determination of EE (ratio between the amount of drugs encapsulated and the total amount of drugs) and LD (ratio between mass

of loaded drugs and total mass of drug-encapsulated nanoparticles), a known amount of CS@AcDXSp, CS@AcDXSp-P or CS@AcDXSp-P-ANP nanoparticles were dissolved in ACN. The CHIR99021 and SB431542 contents were measured by HPLC from the resulting solution, and all the supernatants resulting from the nanoparticle preparation. The *in vitro* release was assessed at pH-values of 7.4 and 5.0, to simulate both the extracellular (pH 7.4) and intracellular (pH 5) microenvironments. The drug-loaded nanoparticles were immersed in the appropriate release medium, stirring at 150 rpm and 37 ± 1°C. Free CHIR99021 and SB431542 were used as controls. Samples of 200 mL were taken at specific time points and analyzed by HPLC, and the same volume of fresh preheated medium was replaced.

Stability in Cell Medium. To evaluate the effect of the cell medium on nanoparticles' hydrodynamic diameter and PdI, 600 µg of nanoparticles were dispersed into 200 µL of freshly prepared Milli-Q-water pH 8. The *Z*-average, PdI, and ζ -potential were measured for $t = 0$, and the nanoparticles were dispersed in 1 mL of complete Dulbecco's Modified Eagle's Medium (DMEM-F12) medium. Samples of 200 µL were diluted into 800 µL of Milli-Q water (pH 8) and measured at 10, 30, 60, 90 and 120 min.

Isolation of Primary Cardiac Cells from Neonatal Rats. Primary cardiac cells were isolated as previously described.[51] Neonatal Wistar rats (1–4 days old) were sacrificed by decapitation, hearts taken, and atrial tissues were discarded. The ventricles were cut into small pieces and enzymatically digested by incubating at 37 °C with gentle mixing for 1:45 h in a collagenase/pancreatin (2 mg/mL). The cells in suspension were collected by centrifugation at 160*g* for 5 min. The supernatant and the top layer containing damaged cells were discarded, and the remaining cells were suspended in DMEM/F12 (Gibco) supplemented with 2.5 mM L-glutamine, 1% of penicillin-streptomycin (PS, HyClone™) and 10% fetal bovine serum (FBS, HyClone™). The cells were pre-plated for about 1:20h to separate cardiomyocytes from non-myocytes,[52] whereafter the unattached cardiomyocytes were plated at a desired density for experiments. After 24 h, the cardiomyocyte medium was replaced with complete serum-free medium (CSFM, DMEM/F12, 2.5 mg/mL bovine serum albumin (BSA, Sigma), 1 µM

insulin, 2.5 mM L-glutamine, 32 nM selenium, 2.8 mM sodium pyruvate, 5.64 μg/mL transferrin, 1 nM T3, and 1% PS). Non-myocytes were cultured in complete DMEM/F12 until confluent and plated for the experiments. On the following day, the medium was changed to serum-free DMEM + 1% PS, 18 h prior to experiments, and these conditions were maintained during the experiments. The cells were maintained at 37 °C with 5% CO_2 and 95% air in a humidified atmosphere.

Cell Viability Studies. The cellular viability of non-myocytes was evaluated using a luminescence assay. Cardiac non-myocytes were seeded at densities of 1×10^4 cells/well in 96-well plates (Corning, USA), and allowed to attach overnight. Nanoparticle suspensions were prepared at different concentrations (10, 25, 50, 100, and 250 μg/mL) in DMEM-F12. After incubation at 37 °C for 6 h, the plates were brought to room temperature for 30 min and washed twice with Hank's Balanced Salt Solution (N-[2-hydroxyethyl]piperazine-N′-[2-ethanesulfonic acid]) (HBSS−HEPES, pH 7.4). The assay reagent (CellTiter-Glo®, Promega, USA) was added to each well, the plates were shaken for 2 min, and the luminescence was measured using a Varioskan Flash Multimode Reader (Thermo Fisher Scientific). For cardiomyocytes, the cell viability was measured taking into account the ability to metabolize 3-(4,5-dimethylthiazol-2-yl)-2,5-diphenyltetrazolium bromide (MTT).[53] MTT (Sigma-Aldrich, USA) was prepared in HBSS−HEPES pH 7.4 (2.5 mg/mL), sterile-filtered with a 0.2 μM syringe filter (Millipore) and stored at +4°C for further use. After a 6-h exposure to nanoparticles, MTT was added to the cells at 0.5 mg/mL and incubated for 2.5 h at +37°C. The supernatant was then carefully removed and 100 μL of DMSO were added. The absorbance was measured using a Varioskan Flash Multimode Reader (Thermo Fisher Scientific) at 490 nm. Negative (1% Triton X-100), positive (cell medium) and blank (only Cell-titer reagent or MTT solution) controls were used and treated similarly.

Cell-nanoparticle Interactions. Non-myocytes seeded at a density of 10^5 cells/well were incubated with Alexafluor 488-labeled nanoparticles (25 μg/mL) for 1 h. A pre-treatment with ANP (100 μM) was carried out 30 min before adding the nanoparticles for competitive binding tests, which was kept for the

duration of the nanoparticle exposure. The cells were then washed three times and collected with trypsinization. The measurements were performed using an LSRII flow cytometer (BD Biosciences, USA) with a laser excitation wavelength of 488 nm. To analyze the internalization of nanoparticles, the fluorescence of membrane-associated nanoparticles was quenched by incubating the cells in trypan blue (0.005% v/v). Approximately 10000 events were obtained per sample. The data analysis was performed using FlowJo X 10.0.7r2 software.

Immunostainings and High Content Cell Imaging. Non-myocytes were seeded at a density of 10^4 cells/well in 96-well plates. The nanoparticle suspensions or free drugs were added to each well at concentrations of 1 µM for CHIR99021 and 2.1 µM for SB431542, and incubated for 6 h. Cells were washed twice with PBS and fixed with 4% paraformaldehyde for 20 min. After 3×5 min washes with PBS, cells were permeabilized with 0.1% Triton X-100 for 10 min, washed 3 times with PBS and blocked with 4% FBS in PBS for 45–60 min. Cells then were incubated with primary antibodies (β-catenin (1:200, ab32572, Abcam), Smad3 (1:250, sc-101154, Santa cruz), α-SMA (1:250, A-2547, Sigma) and vimentin (1:200, D21H3, Cell Signaling)) for 60 min at room temperature, shaking at 300 rpm, followed by 3×5 min washes with PBS. Secondary antibodies were added to each well (anti-mouse 488 (1:250, A11029), anti-mouse 647 (1:250, A21236), anti-rabbit 488 (1:200, A11034), anti-rabbit 647 (A31573) (all from Invitrogen, USA) and DAPI, (1:250, Vector Laboratories) and incubated for 45 min at room temperature, shaking at 300 rpm. Cells were washed 3× 5 min with PBS and stored at +4°C until imaging. The images captured using a Cellomics CellInsight high-content analysis platform (Thermo Scientific) with a 10x objective and analyzed simultaneously using a protocol based on *Compartmental Analysis* bioapplication. DAPI staining was used to define the nuclei and a 5-pixel ring around the nuclear mask was used to represent cytoplasm.

Statistical Analysis. Statistical analyses were performed using one-way ANOVA with Tukey-Kramer post hoc test or Student's *t*-test. The levels of significance were set at probabilities of $^{*,\#,\S,\clubsuit}p < 0.05$, $^{**,\#\#}p < 0.01$, and $^{***,\S\S\S}p < 0.001$.

Supporting Information

Supporting Information is available from the Wiley Online Library or from the author.

Acknowledgements

Alexandra Correia is acknowledged for technical support on drug release studies and Dr Gabor Földes (Imperial College London and Semmelweis University Budapest) for expert advice on high-content analysis. M.P.A.F. acknowledges the Drug Research Doctoral Programme of the University of Helsinki for a Ph.D. grant. H.R. acknowledges the Academy of Finland (Grant No. 266661) and the Sigrid Juselius Foundation for financial support. The Tekes large strategic research opening 3i Regeneration (Project No. 40395/13) is acknowledged for funding. H.A.S. acknowledges financial support from the University of Helsinki Research Funds, the Sigrid Juselius Foundation (Grant No. 4704580), and the European Research Council under the European Union's Seventh Framework Programme (FP/2007 – 2013; Grant No. 310892). The authors acknowledge the following core facilities funded by Biocenter Finland: Electron Microscopy Unit of the University of Helsinki for providing the facilities for TEM imaging, and the Light Microscopy Unit of the Institute of Biotechnology for the instrumentation for HCS microscopy.

Received: ((will be filled in by the editorial staff))
Revised: ((will be filled in by the editorial staff))
Published online: ((will be filled in by the editorial staff))

Pharmacological cellular reprogramming is a highly relevant therapeutic strategy towards cardiac regeneration, and the application of nanoparticles in this emerging field has been scarcely explored. Here, a dual-loaded multifunctional and cardiac-specific nanoparticulate system for potential application in cellular reprogramming of non-myocytes into cardiomyocyte-like cells is reported, promoting a pH-triggered drug delivery and modulation of signaling factors involved in cardiac reprogramming.

Keywords: nanoparticles, small drug molecules, atrial natriuretic peptide, targeted drug delivery, heart

Mónica P.A. Ferreira, Virpi Talman, Giulia Torrieri, Dongfei Liu, Gonçalo Marques, Karina Moslova, Zehua Liu, João F. Pinto, Jouni Hirvonen, Heikki Ruskoaho, Hélder A. Santos

Dual-drug delivery using dextran-functionalized nanoparticles targeting cardiac fibroblasts for cellular reprogramming

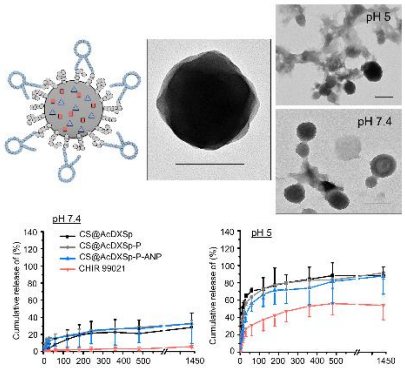

References

[1] World Health Organization, Cardiovascular diseases (CVDs), http://www.who.int/mediacentre/factsheets/fs317/en/, accessed: June, 2017.

[2] E. R. Porrello, A. I. Mahmoud, E. Simpson, J. A. Hill, J. A. Richardson, E. N. Olson, H. A. Sadek, *Science*, **2011**, *331*, 1078.

[3] a) M. Xin, E. N. Olson, R. Bassel-Duby, *Nat. Rev. Mol. Cell Biol.* **2013**, *14*, 529; b) J. P. Cleutjens, W. M. Blankesteijn, M. J. Daemen, J. F. Smits, *Cardiovasc. Res.* **1999**, *44*, 232; c) S. R. Houser, K. B. Margulies, A. M. Murphy, F. G. Spinale, G. S. Francis, S. D. Prabhu, H. A. Rockman, D. A. Kass, J. D. Molkentin, M. A. Sussman, W. J. Koch, *Circ. Res.* **2012**, *111*, 131; d) V. Talman, H. Ruskoaho, *Cell Tissue Res.* **2016**, *365*, 563.

[4] a) M. M. Gaffney, S. O. Hynes, F. Barry, T. O'Brien, *Br. J. Pharmacol.* **2007**, *152*, 175; b) P. N. Matkar, H. Leong-Poi, K. K. Singh, *Gene Ther.* **2016**, *23*, 635; c) J. A. Wolfram, J. K. Donahue, *J. Am. Heart Assoc.* **2013**, *2*; d) A. Raso, E. Dirkx, *Non-coding RNA Res.* **2017**, *2*, 27.

[5] a) V. F. Segers, R. T. Lee, *Nature* **2008**, *451*, 937; b) R. Sun, X. Li, M. I. N. Liu, Y. I. Zeng, S. Chen, P. Zhang, *Int. J. Mol. Med.* **2016**, *38*, 23; c) Y. Haraguchi, T. Shimizu, M. Yamato, T. Okano, *Stem Cells Transl. Med.* **2012**, *1*, 136; d) M. J. Hernandez, K. L. Christman, *JACC Basic Transl. Sci.* **2017**, *2*, 212.

[6] V. F. M. Segers, R. T. Lee, *J. Cardiovasc. Transl. Res.* **2010**, *3*, 469.

[7] a) K. Takahashi, S. Yamanaka, *Cell* **2006**, *126*, 663; b) K. Song, Y.-J. Nam, X. Luo, X. Qi, W. Tan, G. N. Huang, A. Acharya, C. L. Smith, M. D. Tallquist, E. G. Neilson, J. A. Hill, R. Bassel-Duby, E. N. Olson, *Nature* **2012**, *485*, 599.

[8] a) A. N. Patel, T. D. Henry, A. A. Quyyumi, G. L. Schaer, R. D. Anderson, C. Toma, C. East, A. E. Remmers, J. Goodrich, A. S. Desai, D. Recker, A. DeMaria, *Lancet* **2016**, *387*, 2412; b) R. Bolli, A. R. Chugh, D. D'Amario, J. H. Loughran, M. F. Stoddard, S. Ikram, G. M. Beache, S. G. Wagner, A. Leri, T. Hosoda, F. Sanada, J. B. Elmore, P. Goichberg, D. Cappetta, N. K. Solankhi, I. Fahsah, D. G. Rokosh, M. S. Slaughter, J. Kajstura, P. Anversa, *Lancet* **2011**, *378*, 1847; c) K. Malliaras, R. R. Makkar, R. R. Smith, K. Cheng, E. Wu, R. O. Bonow, L. Marbán, A. Mendizabal, E. Cingolani, P. V. Johnston, G. Gerstenblith, K. H. Schuleri, A. C. Lardo, E. Marbán, *J. Am. Coll. Cardiol.* **2014**, *63*, 110.

[9] K. Rodgers, A. Papinska, N. Mordwinkin, *Ad. Drug Deliv. Rev.* **2016**, *96*, 245.

[10] L. Drowley, C. Koonce, S. Peel, A. Jonebring, A. T. Plowright, S. J. Kattman, H. Andersson, B. Anson, B. J. Swanson, Q. D. Wang, G. Brolen, *Stem Cells Transl. Med.* **2016**, *5*, 164.

[11] a) X. Lian, J. Zhang, S. M. Azarin, K. Zhu, L. B. Hazeltine, X. Bao, C. Hsiao, T. J. Kamp, S. P. Palecek, *Nat. Protoc.* **2013**, *8*, 162; b) D. M. Titmarsh, N. R. Glass, R. J. Mills, A. Hidalgo, E. J. Wolvetang, E. R. Porrello, J. E. Hudson, J. J. Cooper-White, *Sci. Rep.* **2016**, *6*, 24637.

[12] Y. Zhao, P. Londono, Y. Cao, E. J. Sharpe, C. Proenza, R. O'Rourke, K. L. Jones, M. Y. Jeong, L. A. Walker, P. M. Buttrick, T. A. McKinsey, K. Song, *Nat. Commun.* **2015**, *6*, 8243.

[13] G. J. Inman, F. J. Nicolas, J. F. Callahan, J. D. Harling, L. M. Gaster, A. D. Reith, N. J. Laping, C. S. Hill, *Mol. Pharmacol.* **2002**, *62*, 65.

[14] J. L. Ifkovits, R. C. Addis, J. A. Epstein, J. D. Gearhart, *PLoS One* **2014**, *9*, e89678.

[15] S. L. Paige, T. Osugi, O. K. Afanasiev, L. Pabon, H. Reinecke, C. E. Murry, *PLoS One* **2010**, *5*, e11134.

[16] G. Ozhan, G. Weidinger, *Cell Regen.* **2015**, *4*, 3.

[17] H. Wang, N. Cao, C. I. Spencer, B. Nie, T. Ma, T. Xu, Y. Zhang, X. Wang, D. Srivastava, S. Ding, *Cell Rep.* **2014**, *6*, 951.

[18] M. P. A. Ferreira, V. Balasubramanian, J. Hirvonen, H. Ruskoaho, H. A. Santos, *Curr. Drug Targets* **2015**, *16*, 1682.

[19] a) A. Patel, M. Patel, X. Yang, A. K. Mitra, *Protein Pept. Lett.* **2014**, *21*, 1102; b) B. P. Yan Teck Ho, Hames Chen Yong Kah, *Nanomedicine* **2016**, *11*, 693.

[20] a) F. R. Formiga, B. Pelacho, E. Garbayo, G. Abizanda, J. J. Gavira, T. Simon-Yarza, M. Mazo, E. Tamayo, C. Jauquicoa, C. Ortiz-de-Solorzano, F. Prósper, M. J. Blanco-Prieto, *J. Control. Release* **2010**, *147*, 30; b) M.-Y. Chang, Y.-J. Yang, C.-H. Chang, A. C. L. Tang, W.-Y. Liao, F.-Y. Cheng, C.-S. Yeh, J. J. Lai, P. S. Stayton, P. C. H. Hsieh, *J. Control. Release* **2013**, *170*, 287; c) F. R. Formiga, B. Pelacho, E. Garbayo, I. Imbuluzqueta, P. Díaz-Herráez, G. Abizanda, J. J. Gavira, T. Simón-Yarza, E. Albiasu, E. Tamayo, F. Prósper, M. J. Blanco-Prieto, *J. Control. Release* **2014**, *173*, 132.

[21] T. Heinze, T. Liebert, B. Heublein, S. Hornig, *Polysaccharides II*, Springer, Berlin Heidelberg, Germany, **2006**.

[22] a) S. L. Suarez, A. Muñoz, A. C. Mitchell, R. L. Braden, C. Luo, J. R. Cochran, A. Almutairi, K. L. Christman, *ACS Biomater. Sci. Eng.* **2016**, *2*, 197; b) S. Suarez, G. N. Grover, R. L. Braden, K. L. Christman, A. Almutairi, *Biomacromol.* **2013**, *14*, 3927.

[23] M. P. A. Ferreira, S. Ranjan, S. Kinnunen, A. Correia, V. Talman, E. Mäkilä, B. Barrios-Lopez, M. Kemell, V. Balasubramanian, J. Salonen, J. Hirvonen, H. Ruskoaho, A. J. Airaksinen, H. A. Santos, *Small* **2017**, *13*, 1701276.

[24] a) Y. Chen, Z. Yang, Z.-A. Zhao, Z. Shen, *Stem Cell Res. Ther.* **2017**, *8*, 118; b) J. A. Efe, S. Hilcove, J. Kim, H. Zhou, K. Ouyang, G. Wang, J. Chen, S. Ding, *Nat. Cell Biol.* **2011**, *13*, 215; c) L. Qian, D. Srivastava, *Circ. Res.* **2013**, *113*.

[25] N. Cao, Y. Huang, J. Zheng, C. I. Spencer, Y. Zhang, J. D. Fu, B. Nie, M. Xie, M. Zhang, H. Wang, T. Ma, T. Xu, G. Shi, D. Srivastava, S. Ding, *Science* **2016**, *352*, 1216.

[26] a) F. Fontana, M.-A. Shahbazi, D. Liu, H. Zhang, E. Mäkilä, J. Salonen, J. T. Hirvonen, H. A. Santos, *Adv. Mat.* **2017**, *29*, 1603239; b) H. Zhang, D. Liu, L. Wang, Z. Liu, R. Wu, A. Janoniene, M. Ma, G. Pan, L. Baranauskiene, L. Zhang, W. Cui, V. Petrikaite, D. Matulis, H. Zhao, J. Pan, H. A. Santos, *Adv. Healthc. Mat.* **2017**, *6*, 1601406.

[27] J. V. Jokerst, T. Lobovkina, R. N. Zare, S. S. Gambhir, *Nanomedicine* **2011**, *6*, 715.

[28] a) M. E. Hystad, E. Oie, H. K. Grogaard, K. Kuusnemi, O. Vuolteenaho, H. Attramadal, C. Hall, *Scand. J. Clin. Lab. Invest.* **2001**, *61*, 139; b) X. Lin, J. Hänze, F. Heese, R. Sodmann, R. E. Lang, *Circ. Res.* **1995**, *77*, 750.

[29] K. J. Kauffman, N. Kanthamneni, S. A. Meenach, B. C. Pierson, E. M. Bachelder, K. M. Ainslie, *Int. J. Pharm.* **2012**, *422*, 356.

[30] a) A. Vonarbourg, C. Passirani, P. Saulnier, J. P. Benoit, *Biomaterials* **2006**, *27*, 4356; b) J. S. Suk, Q. Xu, N. Kim, J. Hanes, L. M. Ensign, *Adv. Drug Deliv. Rev.* **2016**, *99*, 28.

[31] L. Kou, J. Sun, Y. Zhai, Z. He, *Asian J. Pharm. Sci.* **2013**, *8*, 1.

[32] a) E. M. Bachelder, T. T. Beaudette, K. E. Broaders, J. Dashe, J. M. J. Fréchet, *J. Am. Chem. Soc.* **2008**, *130*, 10494; b) E. R. Gillies, A. P. Goodwin, J. M. Frechet, *Bioconj. Chem.* **2004**, *15*, 1254; c) J. L. Cohen, S. Schubert, P. R. Wich, L. Cui, J. A. Cohen, J. L. Mynar, J. M. Frechet, *Bioconj. Chem.* **2011**, *22*, 1056.

[33] a) D. B. Ring, K. W. Johnson, E. J. Henriksen, J. M. Nuss, D. Goff, T. R. Kinnick, S. T. Ma, J. W. Reeder, I. Samuels, T. Slabiak, A. S. Wagman, M. E. Hammond, S. D. Harrison, *Diabetes* **2003**, *52*, 588; b) J. F. Callahan, J. L. Burgess, J. A. Fornwald, L. M. Gaster, J. D. Harling, F. P. Harrington, J. Heer, C. Kwon, R. Lehr, A. Mathur, B. A. Olson, J. Weinstock, N. J. Laping, *J. Med. Chem.* **2002**, *45*, 999.

[34] J. A. Cohen, T. T. Beaudette, J. L. Cohen, K. E. Broaders, E. M. Bachelder, J. M. J. Fréchet, *Adv. Mat.* **2010**, *22*, 3593.

[35] D. Liu, H. Zhang, E. Mäkilä, J. Fan, B. Herranz-Blanco, C.-F. Wang, R. Rosa, A. J. Ribeiro, J. Salonen, J. Hirvonen, H. A. Santos, *Biomaterials* **2015**, *39*, 249.

[36] a) P. B. Garlick, G. K. Radda, P. J. Seeley, *Biochem. J.* **1979**, *184*, 547; b) K. R. Khabbaz, F. Zankoul, K. G. Warner, *Ann. Thorac. Surg.* **2001**, *72*, S2227.

[37] M. Dobaczewski, M. Bujak, N. Li, C. Gonzalez-Quesada, L. H. Mendoza, X.-F. Wang, N. G. Frangogiannis, *Circ. Res.* **2010**, *107*, 418.

[38] E. Fröhlich, *Int. J. Nanomedicine* **2012**, *7*, 5577.

[39] J.-M. Rabanel, P. Hildgen, X. Banquy, *J. Control. Release* **2014**, *185*, 71.

[40] S. R. Saptarshi, A. Duschl, A. L. Lopata, *J. Nanobiotechnology* **2013**, *11*, 26.

[41] L. Cao, D. G. Gardner, *Hypertension* **1995**, *25*, 227.

[42] D. J. Lundy, K. H. Chen, E. K. Toh, P. C. Hsieh, *Sci. Rep.* **2016**, *6*, 25613.

[43] S. M. Weis, *Curr. Opin. Hematol.* **2008**, *15*, 243.

[44] a) H. Takahama, T. Minamino, H. Asanuma, M. Fujita, T. Asai, M. Wakeno, H. Sasaki, H. Kikuchi, K. Hashimoto, N. Oku, M. Asakura, J. Kim, S. Takashima, K. Komamura, M. Sugimachi, N. Mochizuki, M. Kitakaze, *J. Am. Coll. Cardiol.* **2009**, *53*, 709; b) Z. Huang, Y. Song, Z. Pang, B. Zhang, H. Yang, H. Shi, J. Chen, H. Gong, J. Qian, J. Ge, *Int. J. Nanomedicine* **2017**, *12*, 3023.

[45] a) V. Di Mauro, M. Iafisco, N. Salvarani, M. Vacchiano, P. Carullo, G. B. Ramirez-Rodriguez, T. Patricio, A. Tampieri, M. Miragoli, D. Catalucci, *Nanomedicine (Lond.)* **2016**, *11*, 891; b) H. Ma, L. Wang, J. Liu, L. Qian, *Methods Mol. Biol.* **2017**, *1521*, 69.

[46] a) J. A. A. M. Kamps, G. Krenning, *World J. Cardiol.* **2016**, *8*, 163; b) C. L. Hastings, E. T. Roche, E. Ruiz-Hernandez, K. Schenke-Layland, C. J. Walsh, G. P. Duffy, *Adv. Drug Deliv. Rev.* **2015**, *84*, 85.

[47] a) K. Inagawa, K. Miyamoto, H. Yamakawa, N. Muraoka, T. Sadahiro, T. Umei, R. Wada, Y. Katsumata, R. Kaneda, K. Nakade, C. Kurihara, Y. Obata, K. Miyake, K. Fukuda, M. Ieda, *Circ. Res.* **2012**, *111*, 1147; b) T. M. Jayawardena, B. Egemnazarov, E. A. Finch, L. Zhang, J. A. Payne, K. Pandya, Z. Zhang, P. Rosenberg, M. Mirotsou, V. J. Dzau, *Circ. Res.* **2012**, *110*, 1465; c) J. D. Fu, N. R. Stone, L. Liu, C. I. Spencer, L. Qian, Y. Hayashi, P. Delgado-Olguin, S. Ding, B. G. Bruneau, D. Srivastava, *Stem cell Rep.* **2013**, *1*, 235.

[48] A. S. Tseng, F. B. Engel, M. T. Keating, *Chem. Biol.* **2006**, *13*, 957.

[49] a) K. E. Broaders, J. A. Cohen, T. T. Beaudette, E. M. Bachelder, J. M. J. Fréchet, *Proc. Nat. Acad. Sci. U.S.A.* **2009**, *106*, 5497; b) D. Liu, S. Cito, Y. Zhang, C. F. Wang, T. M. Sikanen, H. A. Santos, *Adv. Mat.* **2015**, *27*, 2298.

[50] M. P. A. Ferreira, S. Ranjan, A. M. R. Correia, E. M. Mäkilä, S. M. Kinnunen, H. Zhang, M.-A. Shahbazi, P. V. Almeida, J. J. Salonen, H. J. Ruskoaho, A. J. Airaksinen, J. T. Hirvonen, H. A. Santos, *Biomaterials* **2016**, *94*, 93.

[51] S. Pikkarainen, H. Tokola, T. Majalahti-Palviainen, R. Kerkelä, N. Hautala, S. S. Bhalla, F. Charron, M. Nemer, O. Vuolteenaho, H. Ruskoaho, *J.Biol. Chem.* **2003**, *278*, 23807.

[52] I. S. Polinger, *Exp. Cell Res.* **1970**, *63*, 78.

[53] L. A. Gomez, A. E. Alekseev, L. A. Aleksandrova, P. A. Brady, A. Terzic, *J. Mol. Cell. Cardiol.* **1997**, *29*, 1255.

Click here to access/download
Supporting Information
SI_Revised.docx

Scheme 1

Click here to access/download
Production Data
Scheme 1.tif

Fig. 1

Click here to access/download
Production Data
Figure 1.tif

Fig. 2

Click here to access/download
Production Data
Figure 2.tif

Fig. 3

Click here to access/download
Production Data
Figure3.tif

Fig. 4

Click here to access/download
Production Data
Figure 4.tif

Fig. 5

Click here to access/download
Production Data
Figure 5.tif

ToC

Click here to access/download
Production Data
ToC.tif